High Speed Rotor Drop-Downs in Different Planetary Touch-Down Bearings Differing in the Number of Bearing Units

Benedikt Schüßler[(✉)] and Stephan Rinderknecht

Institute for Mechatronic Systems, Technical University of Darmstadt, Darmstadt, Germany
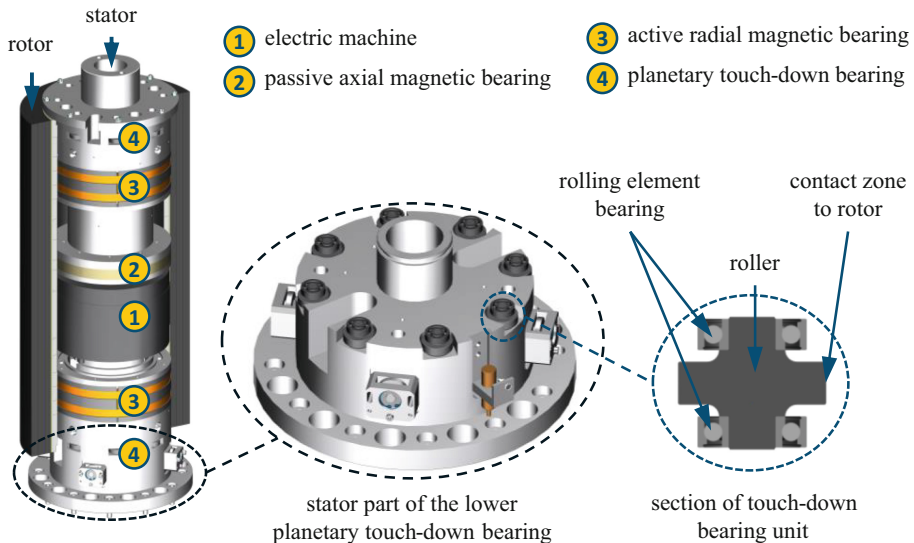{schuessler,rinderknecht}@ims.tu-darmstadt.de

Abstract. The design of touch-down bearings (TDB) for vertical, magnetically levitated outer rotor flywheels with high rotational speeds and operation under vacuum conditions is a challenging task. Conventional TDB are not suited for big diameters with high rotational speeds resulting in surface speeds of above 230 m/s. For such systems, the planetary design can be applied, consisting of several TDB units distributed circumferentially around the stator. This design has the advantages of a decoupling of the rotor diameter from the rolling element bearing diameter as well as a whirl-suppressing characteristic due to the polygonal-shaped clearance. The influence of the number of TDB units on the drop-down behavior is rarely investigated in the literature. However, it is expected that the number of TDB units influences the drop-down behavior and consequently the bearing service life heavily. Therefore, this paper investigates in simulations and experiments drop-downs with six, four, and three TDB units. The simulations are conducted with the simulation software ANEAS. The experiments are conducted with the TDB test rig, which is a robust test rig designed for rotor drop-downs in TDB. The results of both simulation and experiments indicate that the forces on the TDB are lower in configurations with less than six TDB units. However, with three units, the TDB was destroyed the fastest within less than twelve drop-downs.

Keywords: touch-down bearing · drop-down test · drop-down simulation · high-speed drop-down · backup bearing

1 Introduction

Flywheels are energy storage systems with high power in relation to stored energy. Therefore, one possible application is in the electricity grid for grid stabilization and power quality improvement [1]. This becomes even more relevant with more and more renewable energy sources in the electricity grid. However, flywheels can be used not only in the electricity grid but also in industrial applications for example for peak shaving or energy flexibilization [2, 3]. In these applications, money is saved by requiring a lower maximum power or having other systems in a more efficient operating point. The advantages of flywheels are their high lifetime, low maintenance, and applicability in different environments [4–6]. However, for all applications, the efficiency of the system

is of high relevance. To have low losses, modern flywheels are often operated under vacuum conditions and use magnetic bearings to reduce mechanical friction [7, 8]. Up to now, three flywheel systems have been built at the Institute of Mechatronic Systems at TU Darmstadt. Figure 1 shows a section view of the CAD model of the rotor-stator-system for the newest system SWIVT290. The main components of the system are labeled and described in the following.

stator

rotor

1 electric machine

2 passive axial magnetic bearing

3 active radial magnetic bearing

4 planetary touch-down bearing

rolling element bearing

contact zone to rotor

roller

stator part of the lower planetary touch-down bearing

section of touch-down bearing unit

Fig. 1. Section view of the rotor-stator system of the flywheel SWIVT290 without the containment.

To increase the energy stored in the system, it is built as an outer rotor system. The rotor is a hollow cylinder made of fiber-reinforced plastic with metal inserts for the active components. Compared to steel, fiber-reinforced plastic has a higher yield strength and lower weight, which allows higher rotational speeds and consequently a higher stored energy. A comparison of different rotor materials is given in [4]. The rotor is accelerated and decelerated by a permanent synchronous machine. As Fig. 1 shows, it is placed in the middle of the system. This type of electric machine is chosen due to its high conversion efficiency. On top of the electric machine, a passive magnetic bearing for the axial levitation is placed. These two components are surrounded by the active magnetic bearings (AMB) for the radial direction. Since AMB are not fail-safe, touch-down bearings (TDB) are needed to bear the rotor in case of overload or malfunction of the AMB. The TDB are located at the lower and upper end of the system. Figure 2 shows schematically on the left a conventional TDB and on the right a planetary TDB for outer rotor systems. The planetary TDB consists of several small bearing units distributed circumferentially around the stator. Each bearing unit consists of one and two rolling element bearings at the upper and lower end of the roller (see Fig. 1). The outer rings of the rolling element bearings are mounted in the stator. During a drop-down, the roller

gets into contact with the rotor. For both TDB designs in Fig. 2, the rotor is in contact with TDB on the upper right side.
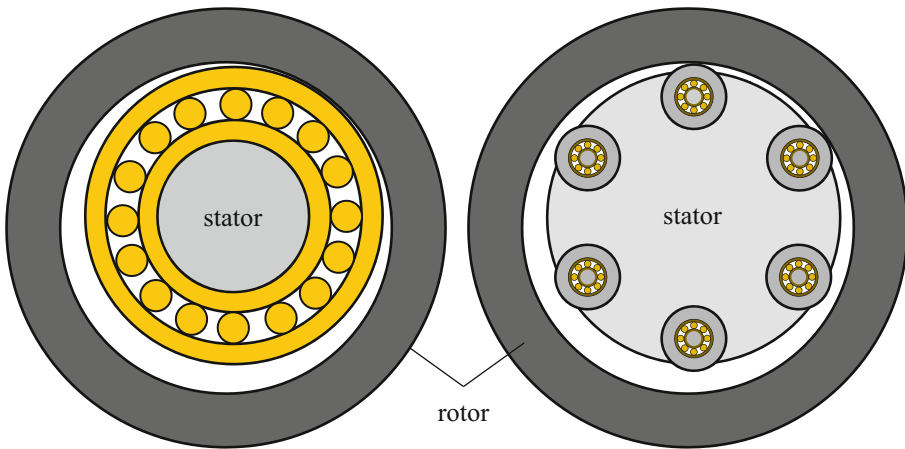
Fig. 2. Schematic representation of a TDB (left: conventional; right: planetary) for an outer rotor system that is in contact with the TDB on the upper right side (not true to scale)

This planetary TDB design has certain advantages compared to conventional TDB. In a conventional TDB for an outer rotor system, the bearing diameter is only slightly smaller than the rotor diameter (see left side of Fig. 2). In a planetary TDB, the bearing diameter is significantly smaller than the rotor diameter and the exact size of the bearings can be chosen independently from the rotor diameter. The rotational speed of the rolling element bearing can thus be influenced by the roller diameter. Vertical rotor systems like the flywheel SWIVT290 have a higher tendency to enter a backward whirl. Hence, the whirl-suppressing characteristic of planetary TDB, which was shown in [9, 10] is a further advantage especially relevant for vertical flywheels. However, planetary TDB have the disadvantage that the used rolling element bearings are comparatively small and consequently have lower load ratings. As a result, it is necessary to reduce the loads as far as possible to reach a high service life of the TDB. The loads on the planetary TDB are influenced by several parameters. One parameter, which is rarely investigated in the literature, is the number of bearing units in the planetary TDB. In [10], the number of TDB units is investigated for low drop-down speeds on an outer rotor flywheel system. The investigated configurations are 8-unit and 6-unit TDB. The results indicate that a whirling motion is more likely to occur with the 8-unit TDB. Consequently, the loads are lower for the 6-unit TDB. In comparison to that, this paper aims to investigate a lower number of TDB units at higher drop-down speeds. The system used for the investigation is the TDB test rig instead of an outer rotor flywheel.

2 Method

The investigation of the influence of the number of units on the drop-down behavior and loads on the TDB is conducted in two steps: firstly, with a simulation study and secondly, with experiments. The test rig used for the experiments is also the basis for the modeling of the simulation study. Therefore, the test rig is described in more detail in Sect. 3. In contrary to the overall goal to build a robust TDB for outer rotor flywheels, the test rig used for this investigation is an inner rotor system. However, it has similar rotodynamic properties to outer rotor flywheels [11, 12].

The effort to investigate a wide range of different numbers of TDB units in planetary TDB with simulations is low compared to real experiments. Therefore, models with 3, 4, 5, 6, 7 and 8 units are derived in the simulation study. Because some parameters are not exactly known or vary from drop-down to drop-down, 24 simulations were conducted for each different TDB configuration. The 24 simulations vary in the initial conditions and some uncertain parameters are varied as well.

For the experimental investigation, test series with three different numbers of units were analyzed. The test rig was built originally with 6-unit TDB. The results of this TDB configuration have already been described in [13]. However, they are also used in this paper for comparison. In addition to the 6-unit TDB, drop-down test series for 3-unit and 4-unit TDB were performed.

3 Test Rig

The TDB test rig is dedicated to drop-down tests. For this purpose, it is built as a robust inner rotor system with an easy exchangeability of components. Another focus of the TDB test rig is the measurement of different values concerning the TDB like forces, temperatures, and rotational speeds. However, it is also designed to mimic the rotodynamic properties of the outer rotor flywheels. Therefore, the system is highly gyroscopic, vertically oriented, and has surface velocities of 230 m/s at the TDB. Since the purpose of the test rig is to test the TDB which may destroy it, the test rig has a secondary TDB for a save spin down even after the primary TDB failed.

3.1 Mechanical Design

Figure 3 shows a model of the test rig, which is used for the investigation in this paper. In the following, the main components are explained and compared to the outer rotor flywheel shown at the beginning in Fig. 1.

Like the flywheels, the rotor is levitated magnetically, and the electric machine is a permanent magnetic synchronous machine. In contrast to the flywheels, also the axial magnetic bearing is an AMB because efficiency is not the main objective of this test rig. The primary TDB plane has similar surface velocities like the flywheels and is made to mount a planetary TDB. Figure 4 shows a more detailed partial section view of the planetary TDB. On the left side of the section view, one can see the TDB unit with structurally integrated strain gauges (strain gauges themselves are not visible). The right side of the section of the planetary TDB shows the TDB unit where the forces are
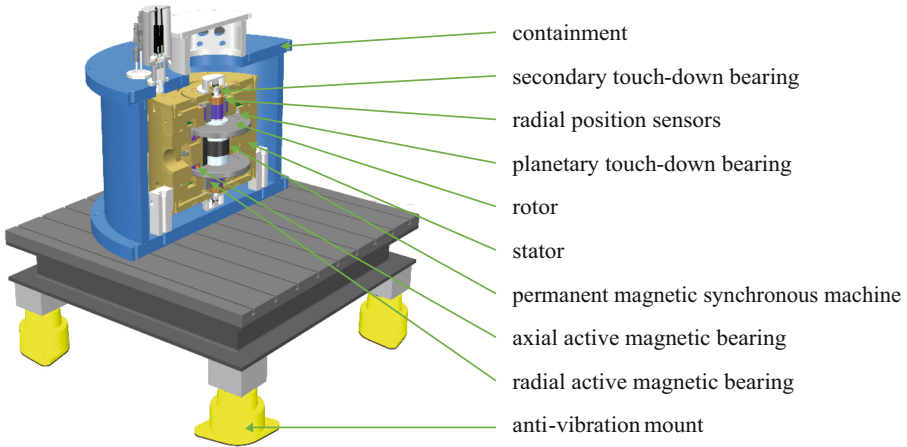
Fig. 3. Partial section view of the TDB test rig.

measured with a piezoelectric force sensor. As in the flywheels, the roller in the TDB unit gets into contact with the rotor during a drop-down. On the upper and lower end are two angular contact bearings. For the experiments shown in this paper, hybrid spindle bearings of type 6001 with vacuum grease were used.
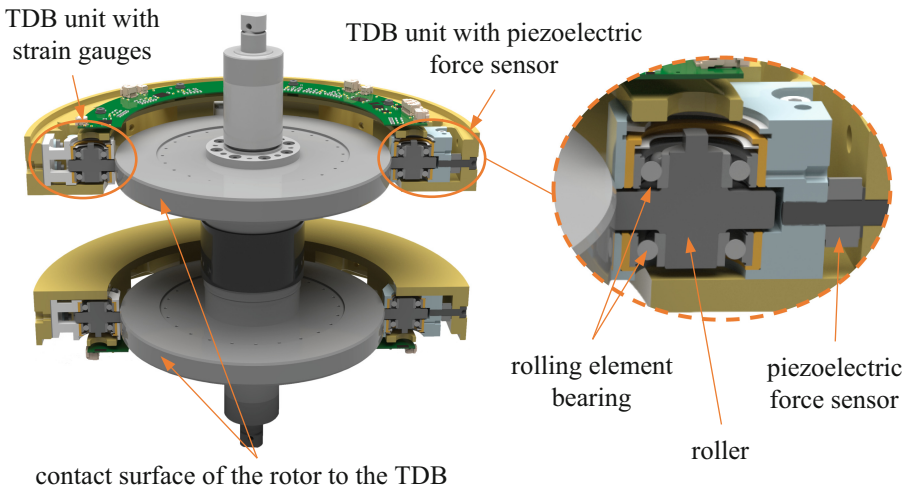

Fig. 4. Partial section view of the planetary TDB and the rotor. Detailed view of the TDB unit for the piezoelectic force measurement.

The secondary TDB is conventional with a single rolling element bearing in each plane and in comparison to the primary TDB, it has much lower surface velocities, due to the smaller radius. The TDB test rig has an inertia of around 0.073 kg m^2 while the SWIVT290 has an inertia of around 5.1 kg m^2. Despite the differences the spin-down

times after a drop-down are comparable since the flywheel decelerates with a braking resistor which is not used during a normal drop-down scenario in the TDB test rig. The TDB test rig decelerates mainly due to friction in the TDB resulting in spin-down times of 3 to 6 min depending on the condition of the TDB. To test the different numbers of TDB units, two different TDB housings have been used, which are shown in Fig. 5: one with 6 pockets and one with 8 pockets. The TDB housing with 6 pockets was used for the test series with the 6-unit TDB and for the test series with the 3-unit TDB in which only every second pocket was equipped with a TDB unit. The TDB housing with 8 pockets was used for the test series with the 4-unit TDB, again only every second pocket was equipped with a TDB unit. The pockets in the 8-pocket housing are bigger than the pockets in the 6-pocket housing. This is because space is needed for the measurement of the forces with strain gauges, which were only used in the test series with 4 TDB units.
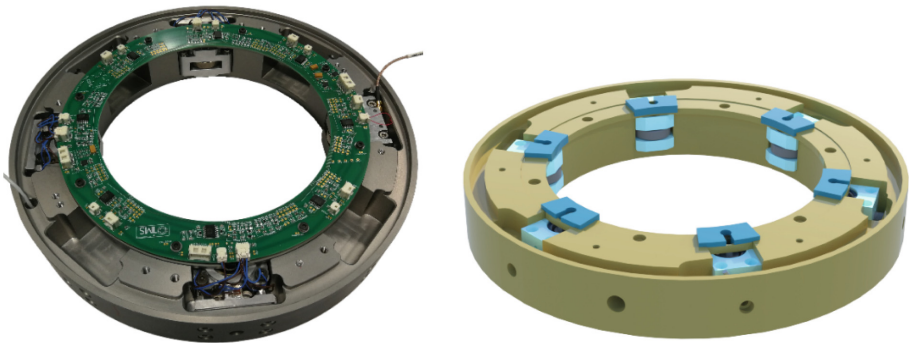
Fig. 5. Two different designs for the housing of the planetary TDB in the TDB test rig (left: 8-pocket housing (real system), right: 6-pocket housing (CAD model)).

3.2 Measurement System

Since the system uses AMB, the position of the rotor is always measured. For the radial direction, four eddy current sensors in each plane are used, enabling a high frequent position measurement. For the axial direction, two inductive position sensors are used. In addition, the TDB test rig is equipped with multiple sensors measuring different values concerning the TDB, for example roller speed, bearing temperature and forces on the TDB. With these measurements, a deeper analysis of the drop-downs is possible.

At one TDB unit in each TDB plane, the radial contact force is measured with a piezoelectric force transducer. For the drop-down series with 4-unit TDB, a new TDB housing had to be built. For this revision, the force measurement was extended so that the force is measured at every TDB. The piezoelectric force sensor at one TDB unit in each TDB plane was kept whereas the forces on the remaining TDB units are measured by structurally integrated strain gauges. Both the TDB units with the piezoelectric force sensor and the TDB units with the strain gauges are made of aluminum and have a similar stiffness. At every TDB unit, the rotational speed of the roller is measured as

well as the temperature of the bearing housing. The measurement of the rotational speed is performed by hall sensors giving a signal twice per revolution. The same principle and the same sensors are used to measure the rotor speed. The temperature measurement is performed with PT100 sensors. In the TDB unit with piezoelectric force transducers, the temperature is measured directly at the outer ring of the upper rolling element bearing. In the case of TDB units for force measurement with strain gauges, the temperature is measured by PT100 mounted at the outside of the TDB unit.

Besides these measurements, also the temperatures of the raceways on the rotor in the TDB planes are measured with infrared temperature sensors. Table 1 gives an overview of the installed sensors and their manufacturers.

Table 1. Measured values in the TDB test rig with measurement principle and producer.

| measured value	sensor type	manufacturer (type)
radial position	eddy current	eddylab (T2)
axial position	inductive	Balluff (BAW0033)
TDB temperature	PT100	Thermo Sensor and Heraeus + transducer: LKM (Typ264)
rotor temperature	infrared	Optris (CT 3ML)
force	piezoelectric	PCB (211B); transducer: Kistler (5073A411)
force	strain gauge	Omega (SGD-2/350-XY13)
rotational speed	hall-effect	Allegro (TS667LSH)

For the data acquisition, a measuring system from National Instruments is used. For the acquisition of the signal from the hall sensor, counter inputs of measurement cards of type NI PCIe-6612 are used. The other signals are measured with cards of type NI PCI 6251, NI PCI 6225 and NI PCI 6229. The configuration was changed for the test series with 4 TDB units due to the additional signals of the strain gauge measurement. Therefore, also the assignment of the data acquisition cards to the signals was changed. The position and force measurements with the piezoelectric sensor were always measured with a frequency of 8 kHz. The forces based on the strain gauges were measured with 6 kHz. The measurement frequency of the temperature was at least 100 Hz.

4   Modeling

The simulations are conducted with the MATLAB-based simulation software ANEAS (Analysis of Nonlinear Active Magnetic Bearing Systems), which has been developed at the Institute for Mechatronic Systems at TU Darmstadt. The software can be used to investigate the behavior of systems levitated with AMB. Especially the case of drop-downs can be simulated. First, Orth [14] developed the software to investigate the drop-down behavior of inner rotor system in conventional bearing systems. Later, it was extended to also investigate the drop-down behavior in planetary TDB, firstly for inner

rotor systems but later on also for outer rotor systems [12, 15]. However, only radial movements can be investigated with the simulation software.

The model consists of a flexible rotor and a flexible stator model. The models are finite element models consisting of 1D Timoshenko beam elements. Figure 6 shows on the left the FE model of the rotor and on the right of the stator. The light grey elements are the elements that have stiffness as well as mass. The dark grey elements in comparison have only mass and do not contribute to the stiffness. For example, the motor windings and the potting around them are not expected to contribute significantly to the overall stiffness. Nodes are marked as circles. The yellow x marks the node that is placed in the center of gravity. The green diamond marks the node where the position sensor is placed. The red diamond marks the node where the TDB is placed and which is therefore important for the following calculations.
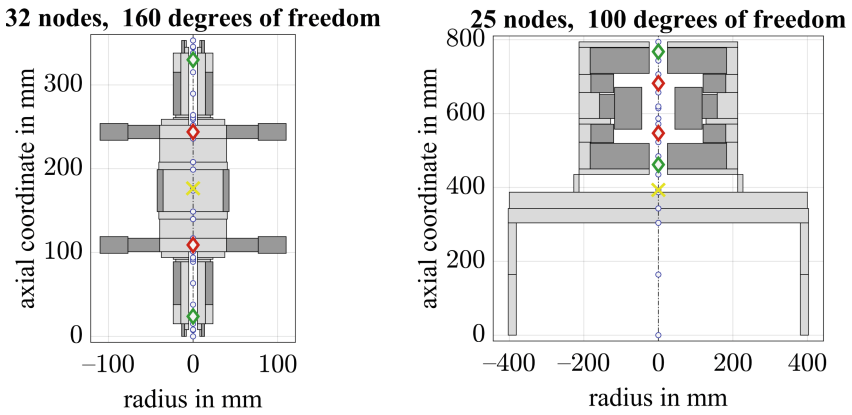
Fig. 6. Schematics of finite element model of rotor (left) and stator (right) of TDB test rig.

The rotor model has 32 nodes. For the rotor, every node has 5 degrees of freedom. Two lateral movements and three rotational movements are possible for the rotor nodes. The stator model has 25 nodes and every node has only four degrees of freedom. The rotational degree of freedom around the longitudinal axis is neglected since the stator does not rotate and the small rotations resulting from contacts are neglected. The properties obtained from the finite element model are then used as parameters for the equation of motion. Equation 1 shows the general equation of motion, which is used for the modeling. The rotational speed of the rotor is given by Ω. q are the displacements and tilting angles in the absolute frame. Furthermore, M is the mass matrix, K the stiffness matrix, ΩG the gyroscopic matrix. The matrix for the inner and outer Damping are expressed by D_{in}, D_{in}^* and D_{out}. The external forces are on the right side of the equation.

$$M\ddot{q} + (D_{out} + D_{in} + \Omega G)\dot{q} + (K - \Omega D_{in}^*)q = f \tag{1}$$

For both the rotor and the stator, a model is built based on the equation of motion shown in Eq. 1. The model of the stator is simpler because it is not rotating and hence there are no gyroscopic effects for the stator. The boundary conditions for the overall system

are that all four degrees of freedom of the node at the bottom of the stator model are fixed, while the rotor is only supported by external forces. The two equations of motion for the stator and the rotor are coupled mainly by contact forces during a drop-down or by magnetic forces during levitation. In addition to these forces, there are minor forces resulting from the permanent magnets of the electric machine which lead to a negative stiffness in the system. During a drop-down, the nonlinear contact forces have the highest relevance and therefore are described in more detail. On the left in Fig. 1, the stiffnesses considered for the stiffness calculation are marked in the section view of the TDB unit. On the right, the equivalent diagram of the stiffnesses is shown. The stiffness of the TDB unit is mainly determined by the stiffness of the rolling element bearing $k_{bearing}$ and the contact stiffness $k_{contact}$ between the rotor-roller contact. The deformation of the TDB unit resulting from the normal contact force F_N is calculated based on the rotor position x_{rotor} and stator position x_{stator} (Fig. 7).
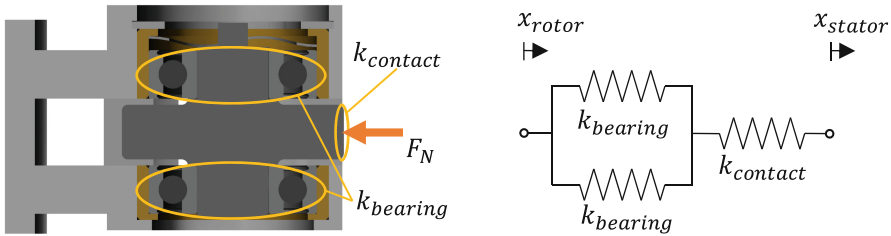
Fig. 7. Left: section view of the TDB unit with strain gauges with considered stiffnesses in the modeling. Right: equivalent diagram of the stiffnesses.

The bearing stiffness is based on the approximation given by Gargiulo and shown in Eq. 2 [16]. $F_{N\_bearing}$ is the normal force acting on the bearing, Z the number of balls, D_m the mean bearing diameter, β the contact angle of the angular contact bearing and $\delta_{bearing}$ the deflection of the bearing.

$$k_{bearing} = \frac{dF_{N\_bearing}}{d\delta_{bearing}} = 3.312 \cdot 10^{10} Z \sqrt{D_m(\cos(\beta))^5 \delta_{bearing}} \tag{2}$$

The contact stiffness between the rotor and the roller results from the deformation of the two concave bodies during contact. For the approximation of this stiffness, the deformation-force relation from Goldsmith is used and shown in Eq. 3 [17]. This equation gives a slightly nonlinear relation between the contact deformation $\delta_{contact}$ and the acting normal force. The radius of the contacting bodies is given by R and the contact length by L. The calculation for the equivalent Young's modulus E^* is given in Eq. 4 where ν is the Poissons ratio and E the Young's modulus.

$$\delta_{contact} = \frac{F_N}{L \pi E^*}\left(ln\left(\frac{L \pi E^*(R_{rotor} + R_{roller})}{F_N R_{rotor} R_{roller}}\right) + 1\right) \tag{3}$$

$$E^* = \frac{1}{\frac{1-\nu_{rotor}^2}{E_{rotor}} + \frac{1-\nu_{roller}^2}{E_{roller}}} \tag{4}$$

For the overall stiffness calculation, it is assumed that the stiffness is equally distributed on both bearings in the TDB unit. With this assumption, the overall TDB stiffness k_{static} is calculated as a sequence of the bearing stiffnesses and the contact stiffness. For the dissipative part of the contact force, the generic model of Hunt and Crossley is applied, which is shown in Eq. 5. δ is the deformation of the overall contact and respectively $\dot{\delta}$ is the contact velocity of the overall contact. The advantage of this damping model is that it is continuous and produces only positive contact forces for low and medium damping factors [18].

$$F_N = k_{static}\delta(1 + \alpha\dot{\delta}) \tag{5}$$

The damping coefficient α is based on the coefficient of restitution (*COR*) and the initial contact velocity $\dot{\delta}^-$ of the overall contact. Its calculation is shown in Eq. 6.

$$\alpha = \frac{3(1 - COR)}{2 - \dot{\delta}} \tag{6}$$

5 Results

In this chapter, the investigation results for the influence of the number of TDB units on the loads acting on the TDB during drop-downs are presented. First, the results of a simulation study based on the previously described model in ANEAS are presented. Afterward, the experimental results from the test series with three different TDB designs are presented. In each test series, a planetary TDB configuration was tested until failure.

5.1 Simulation Results

In the simulation study, TDB configurations between three and eight units are investigated. Because some model parameters or initial conditions are not exactly known, these parameters are varied as well. The varied parameters and their values are given in Table 2. The selected values for the COR are based on literature values given in [19, 20]. The unbalance values are in the range calculated from the unbalance orbit in the measurements. For the drop-down simulations, only the maximum speed of the test rig of 20,000 rpm is investigated because for this speed the highest loads are expected. Therefore, for every number of TDB units, 24 simulations were conducted. At the beginning of a drop-down, all bearings are at standstill. The rotor accelerates the rollers in the TDB units during the contacts until a synchronous rotational speed of the rotor and the rollers is reached. Due to the initially high relative velocity between the rotor surface and the roller surface, these contacts result in high tangential friction forces which lead to a fast rotor movement. When the bearings are accelerated to the synchronous rotor speed, the friction forces decrease due to the equal surface velocity. Because this synchronization happens in the first seconds of the drop-down, a simulation time of 10 s is used for all simulations.

For the comparison and evaluation of the different simulations, severity indicators are used. The rolling element bearings in the planetary TDB are comparatively small

Table 2. Varied parameters in the simulation study.

parameter	values
number of TDB units	3; 4; 5; 6; 7; 8
COR	0.6; 0.7; 0.8
friction coefficient in the bearing	0.0039; 0.0117
unbalance	0.1124 kg mm; 0.2248 kg mm
initial translational velocity	0.01 m/s; 0.05 m/s

to the overall system. It is likely that the amplitude of forces during a drop-down is in the range of the load rating of the bearing and that a single contact damages the bearing permanently. As a result, the maximal normal force F_{max} on the TDB is used as one severity indicator. Another severity indicator not only taking a single value into account but the whole drop-down duration is the calculated bearing service life L_{10}. The bearing service life is based on the rotational speed of the bearing and the normal force in every time step. The TDB consists of multiple rolling element bearings for which the bearing service life is calculated. The bearing service life of the overall TDB $L_{10,min}$ is the minimal bearing service life out of all bearings. The bearing service life calculated for drop-downs is much higher than the actual service life of the TDB. However, even if the calculated value itself is not realistic, it is expected that the bearing service life can be used to compare different drop-downs to each other. If more bearing units are used in the TDB, the costs are higher. Therefore, this paper uses the relative bearing service life $L_{10,min,rel}$, which is the bearing service life in relation to the deployed bearings in the configuration.

In Fig. 8, the results of the simulation study are shown in boxplot diagrams for the two severity indicators maximum force and relative bearing service life. On the left side of Fig. 8, one can see that there is a tendency that the maximum force increases with the number of units in the TDB. The median value of the maximum force is the lowest for
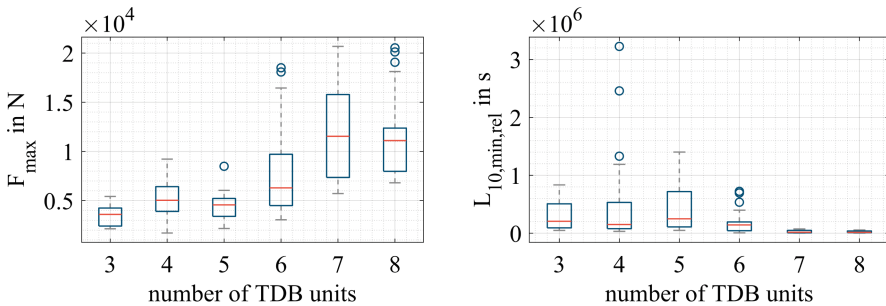
Fig. 8. Box plot diagrams of maximal normal force and relative bearing service life in relation to the number of bearing units in the TDB. The boxes contain 50% of the values in the group, while the whiskers span at maximum the range of 1.5 of the box width. Values outside these ranges are visualized with circles.

the 3-unit TDB with a value of 3,600 N. The highest median value of the maximum force of 11,538 N is reached for the 7-unit TDB but is similar to the 8-unit TDB. Similarly, the median value of the maximum force for the 4-unit TDB is 5,031 N, which is slightly higher than for the 5-unit TDB with 4,571 N. If one looks at the median of the relative bearing service life, the highest value is reached for the 5-unit TDB. However, for the 4-unit TDB, there are some parameter combinations with the highest bearing service life values of all simulations.

5.2 Experimental Results

The test series were performed for TDB with 6, 4, and 3 units. Each test series consists of drop-downs between 5,000 rpm and 20,000 rpm. The drop-down speeds in the different test series were similar. At the beginning of the test series, the drop-down speed was stepwise increased, while later mainly drop-downs at 13,000 rpm and 20,000 rpm were performed. Only if during a drop-down an irregularity occurred, the next drop-down was made at a lower speed. As described in Sect. 3, the forces are measured at every TDB unit only in the test with the 4-unit TDB. Since only the piezoelectric force sensors were present in all test series, the following evaluations are based on these force measurements for a better comparability.

**Results for 6-Unit Touch-Down Bearing**
In Fig. 9, the maximum force measured with the piezoelectric force transducer and the drop-down time duration for the different drop-downs of the test series are shown. It can be seen that the forces are the lowest at the beginning of the test series. In the middle of the test series, the maximum forces rise above 10,000 N. In the second half of the test series, there is a tendency of falling maximum forces. Even at the end of the test series, no high values can be seen in the maximum forces. On the contrary, the drop-down time duration shown on the right of Fig. 9 reaches the highest values at the beginning of the test series where the run down in the TDB needs more than 5 min. After the 8th drop-down, the drop-down duration is between 100 s and 200 s till the 56th drop-down. After that, the drop-down duration decreases to 50 s, which indicates increased friction in the bearings.
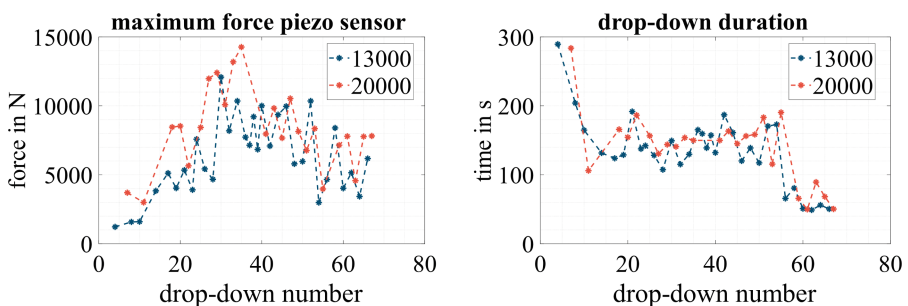
Fig. 9. Maximum force and drop-down duration for the different drop-downs of the test series with the 6-unit TDB.

Results for 4-Unit Touch-Down Bearing

In the test series with the 4-unit TDB, 25 drop-down tests were performed. During the test series, some trouble occurred with the measurement system and the communication with the AMB. As a result, during some drop-downs, the data was not saved or for other drop-downs, also the axial AMB was switched off. For the evaluation, these drop-downs are skipped. However, especially the drop-downs where the axial AMB was switched off led to high forces which may have damaged the bearings considerably. Therefore, the overall number of drop-downs of this test series cannot be compared to the test series with the 6-unit TDB, where no problems occurred. Either way, the number of drop-downs a TDB withstands cannot be determined based on one test series because of probabilities. Nevertheless, Fig. 10 shows the maximum force measured with the piezoelectric force transducer and the drop-down duration for the different drop-downs. The behavior is different from the test series with 6-unit TDB. In the case of the 4-unit TDB, the forces are generally lower. Furthermore, they drastically increase for the last drop-downs of the test series. This has not been noticed for the 6-unit TDB. Moreover, the drop-down durations are different. For the 4-unit TDB, there is a run-in phase where the drop-down duration increases at the beginning of the test series, until it decreases at the last drop-downs before the TDB was destroyed. Generally, the drop-down durations in this test series are higher than in the one shown previously.
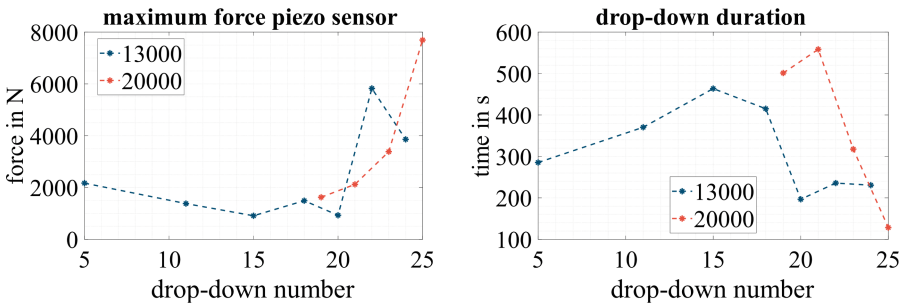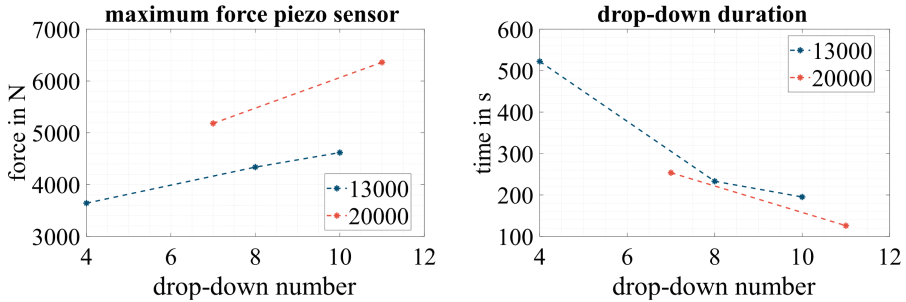

Fig. 10. Maximum force and drop-down duration for the different drop-downs of the test series with the 4-unit TDB.

It can be remarked that the maximum forces measured with the strain gauges which were available in this test series have as expected similar values to the one measured with a piezoelectric force sensor. The highest forces are reached at the beginning of the drop-down when a fast rotor movement occurs and all TDB get into contact with the rotor multiple times. After this phase, the rotor stays more often in one corner of the clearance in this test series. However, during this steady behavior, the forces on the bearings are low and hence this phase does not influence the maximum.

Results for 3-Unit Touch-Down Bearing

To test a TDB with only 3 units, the same housing as in the test series with the 6-unit TDB is used but only every second pocket is equipped with a TDB unit. Due to the increased clearance in the corners, the air gap had to be reduced to half of the one used in the

test series with the 6-unit TDB. In this test series, the TDB was destroyed during the 11th drop-down. This drop-down was the second drop-down from full speed. Figure 11 shows the maximum force measured and the drop-down duration for the different drop-downs with the 3-unit TDB. Again, the forces are lower than in the 6-unit TDB, but they are slightly higher than in the 4-unit TDB. The drop-down durations are similar to the ones seen before. However, there is no run-in phase. From the beginning, the drop-down durations are decreasing and the maximum forces are increasing.

Fig. 11. Maximum force and drop-down duration for the different drop-downs of the first test series with the 3-unit TDB.

The TDB unit which failed during the 11th drop-down was the one equipped with the piezoelectric force sensor. Such an early failure of the TDB has not been expected. To exclude assembly errors or an already damaged bearing, the test series was partly repeated. Therefore, the test rig has been disassembled, the destroyed TDB unit has been changed, and the test rig was assembled again. With the changed TDB unit, the test series was repeated. This time, the TDB was destroyed during the 7th drop-down, which has been the first drop-down from full speed. The same TDB unit as before failed, which was the only one with new rolling element bearings. The maximum measured force was below 5500 N. The situation that both times the same TDB unit failed can be explained by the fact that this TDB unit had the most contact with the rotor. This results from a not aligned geometric and magnetic center. Therefore, the rotor tends to fall more often in one TDB unit, which as a result failed the first.

6   Discussion

In the following, the results from the simulation study and the experiments are discussed. After that, a short comparison of the simulation results with the experimental results is shown.

6.1   Discussion Of Simulation Results

The simulative investigation shows the tendency that lower number of TDB units lead to lower loads on the planetary TDB. These results are in accordance with the literature. In [15, 21], an outer rotor flywheel was dropped in two different planetary TDB

at low speeds. For an 8-unit TDB instead of a 6-unit TDB, the rotor had a higher tendency towards a whirling motion and consequently higher TDB loads. Also in [21], the author showed with simulations that for a planetary TDB, the contact forces rise with an increasing number of TDB units. However, in that investigation, plain bearings were used instead of rolling element bearing and for more than 12 TDB units, the effect reversed. For the present investigation, it was expected that higher number of TDB units lead to higher forces and therefore, it was expected that the highest forces occur for the 8-unit TDB. The results from the simulation study in Fig. 8 show that the highest forces occurred for the 7-unit TDB. This deviation from the tendency that higher numbers of TDB units lead to higher forces can be explained by the relatively low number of simulations and the nearly chaotic behavior of the system. Generally, the analysis of the maximum normal force of the conducted simulations leads to the conclusion that a lower number of bearing units are preferred. However, if one looks at the relative bearing service life (see right side of Fig. 8), which is a severity indicator taking the whole drop-down into account, the 3-unit TDB is not the preferred one. Instead, the most cost-efficient TDB should have 4 or 5 TDB units, depending on if one looks at the median or the highest reached bearing service life values.

6.2 Discussion of Experimental Results

In the test series with the 4-unit TDB, much higher drop-down durations occur than in the test series with the 6-unit TDB. This can be explained by the lower number of bearings, leading to the fact that energy is only dissipated by friction in 4 TDB units instead of 6 TDB units. Apart from this, the rotor stayed more often in one corner of the clearance. As a result, not all TDB units were rotating the whole time, which decreased the losses further and therefore increased the drop-down duration. The same explanation applies to the fact that the first test with 13,000 rpm with the 3-unit TDB had the highest drop-down duration of all experiments at that speed. The experiments after that had shorter drop-down durations. However, this can be explained by already damaged rolling element bearings and therefore higher friction in the bearings which leads to shorter drop-down durations.

The simulations showed that the lifetime of the 3-unit TDB should only be slightly lower than the lifetime of the 4-element TDB. However, the first time the 3-unit TDB failed was at the second experiment from full speed. With the replaced bearing it failed at the first experiment from full speed. One possible explanation for the early failure is the acute angle in the TDB clearance, which results in constraining forces if the rotor surface is uneven. Figure 12 shows a rotor with bumps on the surface in a 3-unit TDB. When the rotor rotates, it can have continuous contact with two bearings. If the bump on the rotor reaches under rotation the first (related to direction of rotation) TDB unit it is in contact with, the bump wants to penetrate the TDB unit as shown in Fig. 12. To avoid this, the rotor has to move away from the TDB unit which hits the bump. However, this movement is partly constrained by the second TDB unit with which the rotor has continuous contact. The bumps can result from material adhesion from the roller material to the rotor material due to previous contacts. The constraining forces resulting from the bumps are not visible in the force measurement due to the high frequency. If such a bump is assumed with a width of 3 mm, the force peaks can reach frequencies up to

70 kHz. However, the force measurement has a low-pass filter with a cutoff frequency of 2 kHz. Therefore, this high frequent force will not be measured with the piezoelectric force sensor.
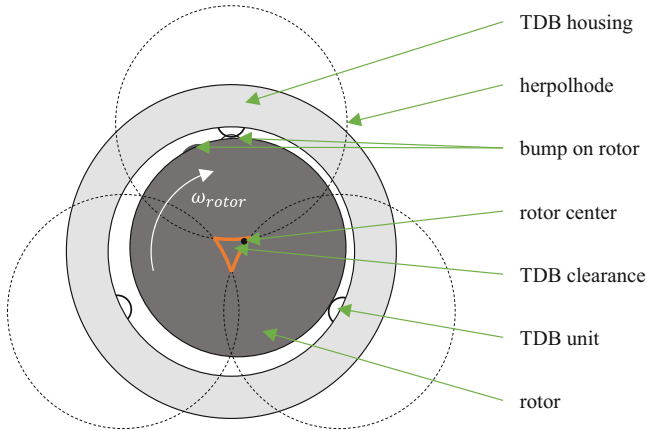
Fig. 12. Rotor with bumps in a 3-unit TDB.

6.3 Comparison of Simulation and Experimental Results

In the simulation study, unknown parameters like the COR or the friction were varied in an expected range. As the boxplot diagram on the left side in Fig. 8 shows, that these parameters have a great influence on the maximum force. For example for the 6-unit, TDB the maximum force varies between 3000 N and 18,500 N. However, this wide range of contact forces is also seen in the experiments. In the experiments with the 6-unit TDB and a drop-down speed of 20,000 rpm, the maximum force varies between 3000 N and 14,425 N. Also for the other test series with the 4- and 3-unit TDB, the measured maximum force is within the simulated range.

From the simulations, it was expected that the 3-unit TDB has only a slightly lower lifetime than the 4-unit TDB. However, the experimental results showed that the 3-unit TDB had a very short lifetime and failed both times in less than two drop-downs from full speed. That difference between simulation and experiment can be explained by the bumps on the rotor in the experiments from previous contacts. In the simulation, the rotor and the roller surface are considered even, hence bumps on the rotor are not modeled. Consequently, in the simulation no constraining forces occur and a higher lifetime is calculated.

7 Conclusion

In the paper, TDB for outer rotor flywheels are investigated. For the investigation of different planetary TDB designs the TDB test rig is used which was described in detail. The analysis consists of a simulation study as well as an experimental analysis. The simulations are analyzed with two severity indicators, the maximum normal force during the drop-down and the relative bearing service life of the TDB. The simulation results indicate:

- that a lower number of units in TDB lead to lower loads on the bearing.
- the highest relative bearing service life can be reached with TDB consisting of 4 or 5 TDB units.

With the TDB test rig, three TDB designs with 3, 4, and 6 units have been investigated. During the test series, the rotor was dropped repeatedly in the planetary TDB until the bearings were destroyed. This led to the following results:

- the highest number of drop-downs without replacing the TDB was reached with the 6-unit TDB.
- the measured forces were lower for the 3- and the 4-unit TDB than for the 6-unit TDB.
- the 3-unit TDB had a short service life. The TDB was destroyed within the second respectively the first drop-down from full speed.
- this was explained with the acute angle in the TDB clearance of the 3-unit TDB. If the surface of the rotor or the TDB is not perfectly round the rotation in one corner of the clearance leads to constraining forces on the TDB units. As a result, acute angles in the TDB clearance should be avoided.

Comparing the simulation results with the experimental results, it can be concluded that both show that forces on the TDB decrease for lower numbers of TDB units. However, in the simulation, a perfectly even rotor surface is assumed, and in the experiments, high frequent force peaks are not measured due to the low pass filtering. Therefore, the simulation model should be extended to uneven rotor surfaces. In addition, for further drop-down tests, the sampling frequency of the force measurement should be increased and an anti-aliasing low-pass filter with a higher cutoff frequency should be used.

References

1. Lazarewicz, M.L., Rojas, A.: Grid frequency regulation by recycling electrical energy in flywheels. In: IEEE Power Engineering Society General Meeting, 2004. 2004 IEEE Power Engineering Society General Meeting, pp. 2038–2042. IEEE, Denver, CO, USA, 6–10 June 2004. ISBN 0-7803-8465-2
2. Hebner, R., Beno, J., Walls, A.: Flywheel batteries come around again. IEEE Spectr. **39**, 46–51 (2002). https://doi.org/10.1109/6.993788

3. Mouratidis, P., Schüßler, B., Rinderknecht, S.: Hybrid energy storage system consisting of a flywheel and a lithium-ion battery for the provision of primary control reserve. In: 2019 8th International Conference on Renewable Energy Research and Applications (ICRERA). 2019 8th International Conference on Renewable Energy Research and Applications (ICRERA), pp. pp 94–99. IEEE Brasov, Romania, 03–06 Nov 2019. ISBN 978-1-7281-3587-8

4. Bolund, B., Bernhoff, H., Leijon, M.: Flywheel energy and power storage systems. Renew. Sustain. Energy Rev. **11**, 235–258 (2007). https://doi.org/10.1016/j.rser.2005.01.004

5. Liu, H., Jiang, J.: Flywheel energy storage—An upswing technology for energy sustainability. Energy Build. **39**, 599–604 (2007). https://doi.org/10.1016/j.enbuild.2006.10.001

6. Hawkins, L., Mcmullen, P., Larsonneur, R.: Development of an AMB Energy Storage Flywheel for Commercial Application (2005)

7. Li, X.: Evaluation and Design of a Flywheel Energy Storage System. TU Darmstatd (2019)

8. Pena-Alzola, R., Sebastian, R., Quesada, J., Colmenar, A.: Review of flywheel based energy storage systems. In: 2011 International Conference on Power Engineering, Energy and Electrical Drives. 2011 International Conference on Power Engineering, Energy and Electrical Drives (POWERENG), pp. 1–6. IEEE, Malaga, Spain, 11–13 May 2011. ISBN 978-1-4244-9845-1

9. Schüßler, B., Hopf, T., Rinderknecht, S.: Simulative investigation of rubber damper elements for planetary touch-down bearings. Bull. Polish Acad. Sci.: Tech. Sci. **69**, e139615 (2021). https://doi.org/10.24425/bpasts.2021.139615

10. Schüßler, B., Hopf, T., Rinderknecht, S.: Drop-downs of an outer rotor flywheel in different planetary touch-down bearing designs. Actuators **11**(2), 30 (2022). https://doi.org/10.3390/act11020030

11. Quurck, L., Schaede, H., Richter, M., Rinderknecht, S.: High speed backup bearings for outer-rotor-type flywheels – proposed test rig design. In: Proceedings of ISMB 14. International Symposium on Magnetic Bearings, pp. 109–114. Linz, Austria, 11–14 Aug 2014

12. Quurck, L., Franz, D., Schuessler, B., Rinderknecht, S.: Planetary backup bearings for high speed applications and service life estimation methodology. Mech. Eng. J. **4**(5), 17-00010–00017-00010 (2017). https://doi.org/10.1299/mej.17-00010

13. Quurck, L., Viitala, R., Franz, D., Rinderknecht, S.: Planetary backup bearings for flywheel applications. In: Proceedings of ISMB 16. International Symposium on Magnetic Bearings, Beijing, China, 13–17 Aug 2018

14. Orth, M., Nordmann, R.: ANEAS: a modeling tool for nonlinear analysis of active magnetic bearing systems. IFAC Proc. Vol. **35**, 811–816 (2002). https://doi.org/10.1016/S1474-6670(17)34039-9

15. Schüßler, B., Hopf, T., Rinderknecht, S.: Drop-downs of an outer rotor flywheel in different planetary touch-down bearing arrangements. In: Gomes, Alfonso Celso, D.N., Santisteban, J.A., Stephan, R.M. (eds.) Proceedings of ISMB 17. The 17th Internatial Symposium on Magnetic Bearings, Virtual, pp. 255–266. Rio de Janeiro, Brazil (2021)

16. Gargiulo, E.P., Jr.: A simple way to estimate bearing stiffness. Mach. Des. **52**, 107–110 (1980)

17. Goldsmith, W.: Impact: The Theory and Physical Behaviour of Colliding Solids. Edward Arnold, London (1960)

18. Hunt, K.H., Crossley, F.R.E.: Coefficient of restitution interpreted as damping in vibroimpact. J. Appl. Mech. **42**, 440 (1975). https://doi.org/10.1115/1.3423596

19. Brake, M.R.W., Reu, P.L., Aragon, D.S.: A comprehensive set of impact data for common aerospace metals. J. Comput. Nonlinear Dyn. **12**, 515 (2017). https://doi.org/10.1115/1.4036760

20. Marinack, M.C., Musgrave, R.E., Higgs, C.F.: Experimental investigations on the coefficient of restitution of single particles. Tribol. Trans. **56**, 572–580 (2013). https://doi.org/10.1080/10402004.2012.748233

21. Simon, U.: Rotor–Stator–Kontakt in polygonförmigen Fanglagern. Dissertation (2002)